Supporting Information

Assembly of graphene oxide vs. reduced graphene oxide in a phospholipid monolayer at air-water interface

Ajit Seth[1], *Priya Mandal*[1#*], *Prashant Hitaishi*[1], *Rajendra P. Giri*[2§], *Bridget M. Murphy*[2], *and Sajal K. Ghosh*[1*]

[1]*Department of Physics, School of Natural Sciences, Shiv Nadar Institution of Eminence, NH91, Tehsil Dadri, G. B. Nagar, Uttar Pradesh 201314, India.*

[2]*Institut für Experimentelle und Angewandte Physik, Christian-Albrechts-Universität Zu Kiel,24098 Kiel, Germany.*

[3]*Ruprecht-Haensel Laboratory, Kiel University, Kiel D-24118, Germany*

*Correspondence: sajal.ghosh@snu.edu.in (S. K. Ghosh), priya.mandal@ucl.ac.uk (P. Mandal)

[#]Present address: Nanoengineered Systems Laboratory, UCL Mechanical Engineering, University College London, London WC1E7JE, UK.

[§]Present address: Department of Physics, Indian Institute of Technology (ISM) Dhanbad, Jharkhand 826004, India.

1. Characterizations of graphene oxide (GO) and reduced graphene oxide (rGO) flakes:

To confirm the successful synthesis of GO and rGO, various characterization techniques are employed. The X-ray diffraction (XRD) spectra for graphite, GO and rGO are displayed in Figure S1(a). The intense peak of graphite centred at 26.4° corresponds to an interlayer spacing of 3.38 Å. Upon oxidation, this graphitic peak shifted to 10.7° with interlayer spacing d = 8.27 Å due to the intercalation of oxygen functional groups. After reduction by ascorbic acid, the peak at 10.7° completely disappeared and was replaced by a broad peak around $2\theta = 23.1°$, implying a successful reduction of GO to rGO. Figure S1(b) shows the corresponding Fourier Transformation Infrared (FTIR) spectra of the as synthesised GO and rGO flakes. The appearance of characteristics vibration modes centred at 3000-3200 cm^{-1} (O-H), 1615 cm^{-1} (C=C), 1416 cm^{-1} (C-OH), and 1044 cm^{-1} (epoxide C-O-C) confirm the oxidation of graphite. After the reduction process, these functional groups were reduced significantly. This can further be verified from the X-ray photoelectron spectra (XPS) data of GO and rGO flakes shown in Figure S1(c)[1] and Figure S1(d), respectively. The corresponding atomic percentage of oxygen in GO and rGO was determined to be ~ 30% and ~16%, respectively.

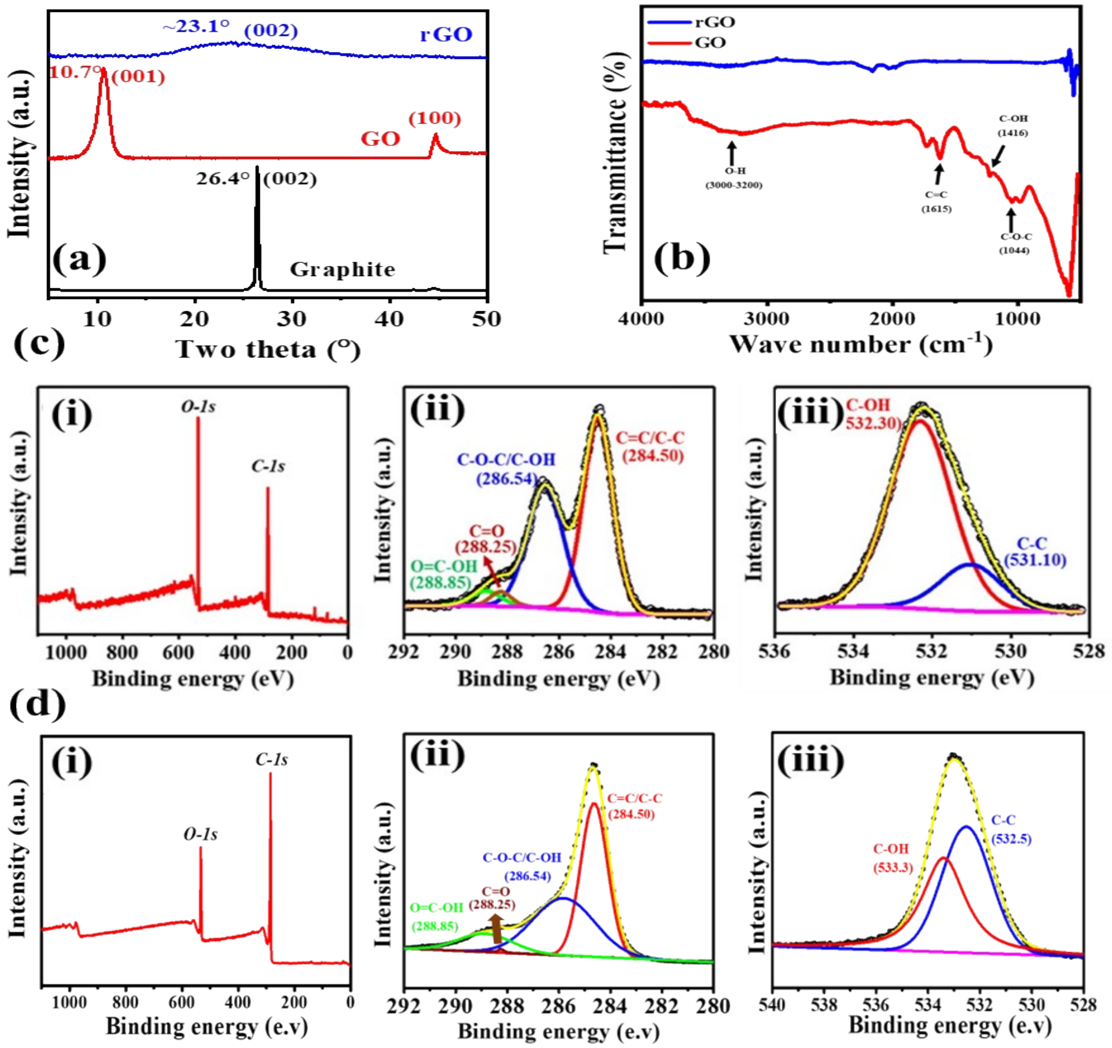

Figure S1. *(a) X-ray diffraction spectra of graphite powder, graphene oxide powder (GO) and reduced graphene oxide powder (rGO); (b) Fourier Transformation Infrared Spectra of graphene oxide (GO) and reduced graphene oxide (rGO); (c) XPS survey analysis and deconvoluted C-1s and O-1s spectra of GO; (d) XPS survey analysis and deconvoluted C-1s and O-1s spectra of Spectra of rGO. Figure S1(c) is reproduced with permission from ref. 1. Copyright Elsevier 2022.*

2. Size of GO and rGO flakes quantified by atomic force microscopy (AFM): Figure S2 shows the atomic force microscopy (AFM) images to quantify the size of GO and rGO nanoflakes. The average size of the GO flakes is found to be 80-200 nm while that of rGO flakes is 250-300 nm.

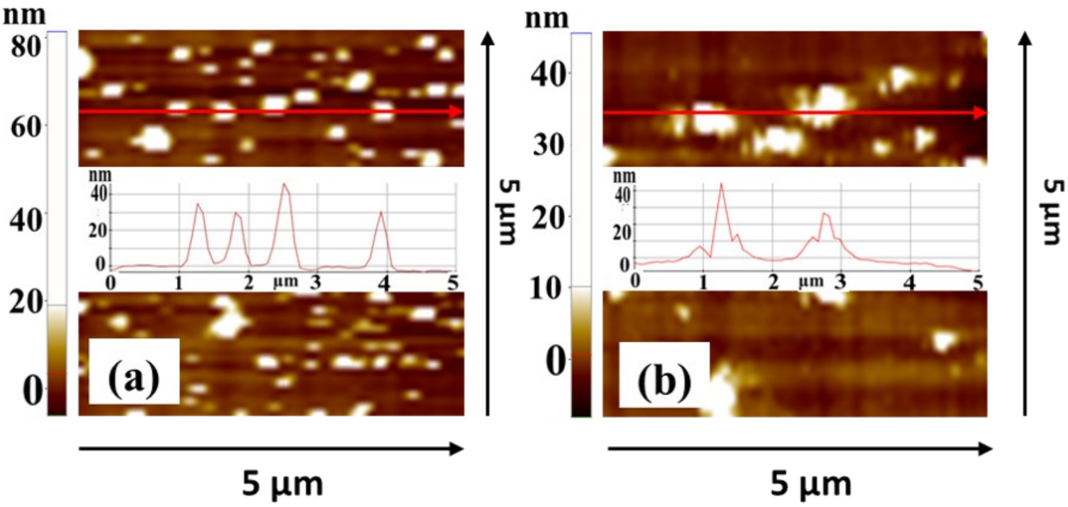

Figure S2: *AFM images of (a) GO, and (b) rGO nanoflakes deposited on silicon wafer and their corresponding height profile.*

3. Measurement of the surface potential of a molecular layer at an air-water interface: The surface potential apparatus is utilized to assess alterations in electric potential (ΔV), which provides important information into molecular orientation at the surface. This measurement relies on the effective dipole moment, derived from the Helmholtz equation,[2] within the framework of a parallel plate condenser model,

$$\Delta V = \frac{\mu_n}{\varepsilon \varepsilon_0 A}$$

where, μ_n represents the vertical component of the dipole moment, ε is the subphase permittivity, and A is the mean area of a molecule at the interface. A Langmuir monolayer can be conceptualized as an array of electric dipoles positioned at the air/water interface. Particularly important are those between the polar groups of lipid molecules and substances dissolved in the subphase (ions or any other soluble molecules). During their interactions, the electrical surface potential of the lipid layer can be decreased or increased[3,4] This measurement of surface potential effectively discerns subtle changes in the electrostatic properties of the surface-active molecules. This is achieved through the utilization of a surface potential sensor (SPOT, KSV NIMA, Biolin Scientific, Sweden). This SPOT sensor quantifies the potential changes across the lipid monolayer by employing a vibrating plate positioned above the monolayer and a submerged counter electrode below in the subphase to detect potential differences.[5] A schematic of the experimental setup is shown in Figure S3 (a). The counter-electrode plate, measuring 35x50x2 mm3, is connected to the measuring device's vibrating head via a cable. The measuring head, with dimensions of 100x85x20 mm3, facilitates simultaneous measurement of surface potential-area isotherms alongside surface pressure-area isotherms, maintaining constant parameters throughout. Figure S3(a) shows the schematic of experimental setup for measuring the surface potential of lipid monolayer formed at air-water interface. Figure S3 (b) and S3 (c) show the surface pressure-area isotherm for GO and rGO subphase and surface potential-area isotherms for GO and rGO subphase, respectively.

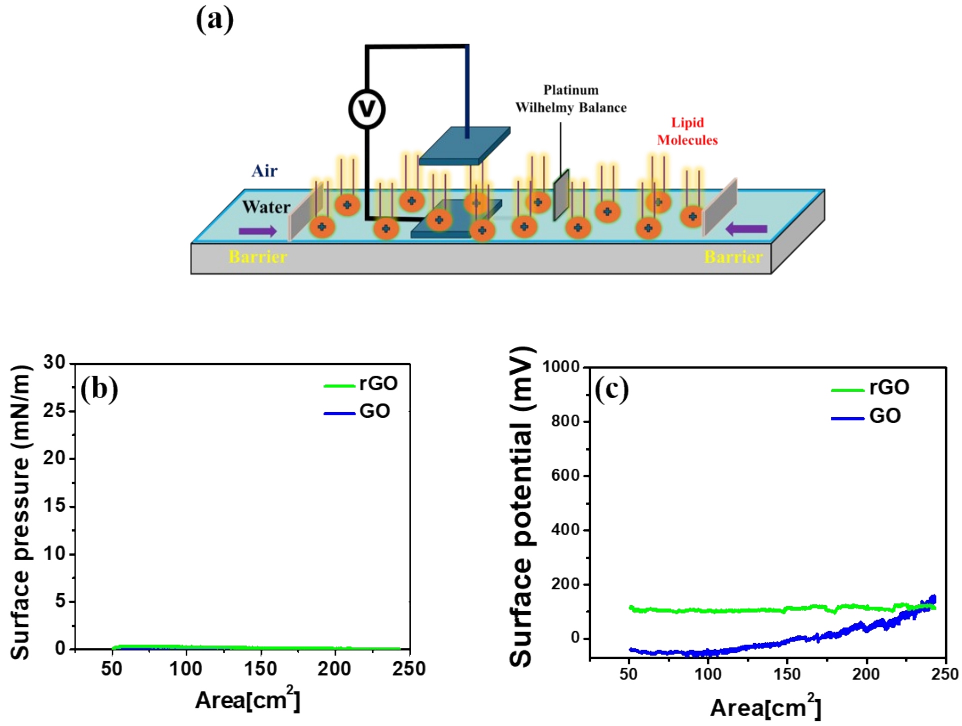

Figure S3 (a): *Schematic of experimental setup for measuring the surface pressure and surface potential of a lipid monolayer formed at air-aqueous interface.* ***(b)*** *Surface pressure-area isotherm for GO and rGO subphase.* ***(c)*** *Surface potential-area isotherms for GO and rGO subphase.*

4. X-ray reflectivity (XRR) data extraction scheme: The schematic of the experimental setup used in the XRR measurements has been discussed in detail in our previous report.[6,7] A python based script has been utilized to extract the 2D images. This process involves integrating the specular intensity by selecting one region of interest (ROI) and two other symmetrically placed ROIs on both sides of the specular one, considering the contributions from background scattering. The background corrected reflectivity profiles were obtained from the integrated intensities as described in ref 6 and ref 7.[6,7] The obtained XRR profiles are further normalized by the Fresnel reflectivity to enhance the present features.[8,9] For this purpose, we simulated a Fresnel reflectivity curve (R_f) by taking the roughness of air-water interface to be 3Å. Then, the final R/R_f curves are obtained by dividing the experimentally collected reflectivity profiles 'R' with the Fresnel reflectivity curves 'R_f'.

5. XRR data analysis scheme: All the XRR data were analysed using Parratt's recursive algorithm in MATLAB. In order to obtain the best fit, two-box and three-box model were used for different layers according to their electron densities across the surface normal. The bottom layer is taken as an infinitely large water layer with fixed interfacial roughness value of 3 Å and the electron density of 0.334 $e^-/Å^3$ for all the samples. The utilization of Parratt's recursive formalism is rooted in Fresnel's theory, where a finite homogeneous slab with a thickness 'd' is employed to describe the reflectivity amplitude, as expressed by the following equation,[10,11]

$$r_{slab} = \frac{r_{01} + r_{12}p^2}{1 + r_{01}r_{12}p^2} \qquad (2)$$

Here, the reflectivity amplitudes at the interfaces 0,1 and 1,2 are denoted as r_{01} and r_{12} and can be obtained through the Fresnel relation, expressed as $r'_{j,j+1} = \frac{Q_j - Q_{j+1}}{Q_j - Q_{j+1}}$, the value of $Q_j = \sqrt{Q^2 - 8k^2\delta_j + i8k^2\beta_j}$ which is defined by the wave vector transfer in the j^{th} layer. Additionally, p^2 is defined as e^{iqd} and represents the phase factor. By utilizing the equation 2, the reflectivity of a homogenous stratified system with N layers can be evaluated using the provided equation,[10,11]

$$r_{slab} = \frac{r_{N-1,N} + r_{N,\infty}p_N^2}{1 + r_{N-1,N}r_{N,\infty}p_N^2} \qquad (3)$$

Additionally, the N^th^ layer offers an environment that facilitates both multiple scattering and refraction, allowing for the occurrence of these processes. Subsequently, by following a similar procedure, the reflectivity from the (N-1)th layer can also be determined as,[6,12]

$$r_{N-2,N-1} = \frac{r_{N-2,N-1} + r_{N-1,N}p_{N-1}^{2}}{1 + r_{N-2,N-1}r_{N-1,N}p_{N-1}^{2}} \quad (4)$$

This procedure can be iteratively extended, ensuring that the reflectivity amplitude (r_{01}) encompassing the interface between vacuum and the first layer is ultimately determined.

6. GIXD diffraction pattern: GIXD is employed to investigate the configuration of lipid chains. This technique involves directing X-rays at a grazing angle onto the sample surface, enhancing sensitivity to surface structures such as lipid layers. The resulting diffraction pattern provides valuable information about the arrangement and orientation of lipid chains in the material. The GIXD pattern obtained from a lipid monolayer consists of characteristics Bragg spots which is attributed to the two-dimensional (2D) ordering of lipid chains. Elaborately, the 2D contour plots, derived from the integration along the q_z and q_{xy} axes, yield Bragg peaks and Bragg rods, respectively. Subsequently, fitting these data involves the application of Lorentzian and Gaussian functions, enabling the extraction of unit cell parameters.

7. Pressure-dependent XRR data of DPPC at air-water interface: The Fresnel normalized XRR profiles of DPPC monolayer dispersed at air-water interface at multiple surface pressures are shown in Figure S4. The corresponding fit parameters are displayed in Table S1. Considering a two-box fitting model for the 10 mN/m case, the thickness of comes out to be 13 Å and 10 Å respectively, while electron density values are 0.357 $e^-/Å^3$ and 0.301 $e^-/Å^3$ respectively. This randomness in the parameters with their unphysical values at low surface pressure indicates inadequate interaction between molecules, leading to no well-organized lipid film. Eventually, with a gradual increase of surface pressure, physically significant values of fitting parameters are obtained, indicating the successful formation of DPPC monolayer.

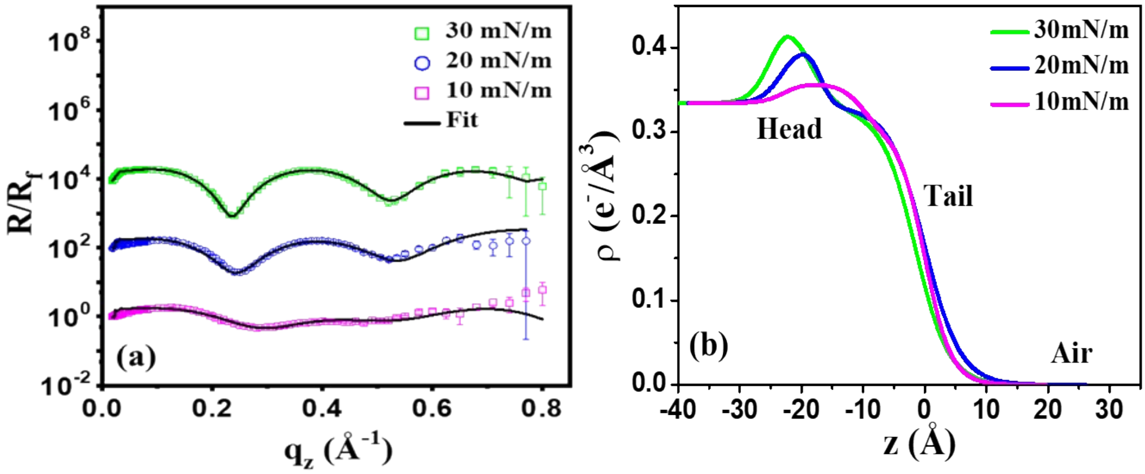

Figure S4. *(a) XRR profiles from DPPC monolayers at air−water interface at different surface pressures. Symbols represent the experimental data whereas the solid lines indicate fits to the data. (b) Corresponding EDPs obtained from the best fit of the reflectivity curve.*

Table S1. *Fit parameters of pressure-dependent XRR data of DPPC monolayer on the water subphase. The parameters d, ρ and σ denote the layer thickness, electron density and the interfacial roughness, respectively.*

Sample	**Pressure**	**Tail**			**Head**		
		d (Å)	**ρ(e⁻/Å³)**	**σ (Å)**	**d (Å)**	**ρ(e⁻/Å³)**	**σ (Å)**
DPPC	30 mN/m	17.6 ± 0.2	0.325 ± 0.007	5.0 ± 0.1	6.2 ± 0.1	0.447 ± 0.012	4.0 ± 0.2
DPPC	20 mN/m	17.0 ± 0.2	0.320 ± 0.007	5.2 ± 0.1	6.2 ± 0.1	0.390 ± 0.010	2.0 ± 0.1
DPPC	10 mN/m	10.0 ± 0.1	0.301 ± 0.007	3.9 ± 0.1	13 ± 0.2	0.357 ± 0.009	3.4 ± 0.2

References:

1 P. Mandal, S. K. Ghosh and H. S. Grewal, Graphene oxide coated aluminium as an efficient antibacterial surface, *Environmental Technology & Innovation*, 2022, **28**, 102591.

2 A. Chachaj-Brekiesz, J. Kobierski, A. Wnętrzak and P. Dynarowicz-Latka, Electrical Properties of Membrane Phospholipids in Langmuir Monolayers, *Membranes*, 2021, **11**, 53.

3 C. B. Casper, D. Verreault, E. M. Adams, W. Hua and H. C. Allen, Surface potential of DPPC monolayers on concentrated aqueous salt solutions, *The Journal of Physical Chemistry B*, 2016, **120**, 2043–2052.

4 G. Luque-Caballero, J. Maldonado-Valderrama, M. Quesada-Pérez and A. Martín-Molina, Interaction of DNA with likely-charged lipid monolayers: An experimental study, *Colloids and Surfaces B: Biointerfaces*, 2019, **178**, 170–176.

5 L. B. Dreier, C. Bernhard, G. Gonella, E. H. G. Backus and M. Bonn, Surface Potential of a Planar Charged Lipid–Water Interface. What Do Vibrating Plate Methods, Second Harmonic and Sum Frequency Measure?, *J. Phys. Chem. Lett.*, 2018, **9**, 5685–5691.

6 P. Mandal, R. P. Giri, B. M. Murphy and S. K. Ghosh, Self-Assembly of Graphene Oxide Nanoflakes in a Lipid Monolayer at the Air–Water Interface, *ACS Applied Materials & Interfaces*, 2021, **13**, 57023–57035.

7 R. Giri, M. Mukhopadhyay, U. Basak, A. Chakrabarti, M. Sanyal, B. Runge and B. Murphy, Continuous uptake or saturation—Investigation of concentration and surface-packing-specific hemin interaction with lipid membranes, *The Journal of Physical Chemistry B*, 2018, **122**, 7547–7554.

8 S. K. Ghosh, S. Castorph, O. Konovalov, T. Salditt, R. Jahn and M. Holt, Measuring Ca2+-Induced Structural Changes in Lipid Monolayers: Implications for Synaptic Vesicle Exocytosis, *Biophysical Journal*, 2012, **102**, 1394–1402.

9 S. K. Ghosh, S. Castorph, O. Konovalov, R. Jahn, M. Holt and T. Salditt, In vitro study of interaction of synaptic vesicles with lipid membranes, *New J. Phys.*, 2010, **12**, 105004.

10 R. P. Giri, A. Chakrabarti and M. K. Mukhopadhyay, Cholesterol-Induced Structural Changes in Saturated Phospholipid Model Membranes Revealed through X-ray Scattering Technique, *J. Phys. Chem. B*, 2017, **121**, 4081–4090.

11 L. G. Parratt, Surface Studies of Solids by Total Reflection of X-Rays, *Phys. Rev.*, 1954, **95**, 359–369.

12 J. Als-Nielsen and D. McMorrow, *Elements of Modern X-ray Physics*, John Wiley & Sons, 2011.